Smart Mater. Struct. **16** (2007) 323–331 doi:10.1088/0964-1726/16/2/010

Identification of electromechanical modal parameters of linear piezoelectric structures

M Porfiri[1], C Maurini[2] and J Pouget[2]

[1] Department of Mechanical, Aerospace and Manufacturing Engineering, Polytechnic University, Brooklyn, NY 11201, USA
[2] Institut Jean Le Rond d'Alembert CNRS (UMR7190), Université Pierre et Marie Curie-Paris 6, 4 Place Jussieu, F-75252 Paris Cedex 05, France

E-mail: mporfiri@poly.edu, maurini@lmm.jussieu.fr and pouget@lmm.jussieu.fr

Received 28 June 2006, in final form 27 November 2006
Published 30 January 2007
Online at stacks.iop.org/SMS/16/323

Abstract
Reduced-order modal models of linear piezoelectric structures are useful in vibration control and health monitoring. We study experimental identification of the fundamental parameters of these modal models. We propose two identification techniques for estimating piezoelectric modal couplings and piezoelectric modal capacitances. Both methods are easily implementable and rely on elementary vibration tests. We show the application of these methods to a sample structure hosting multiple transducers.

(Some figures in this article are in colour only in the electronic version)

1. Introduction

Piezoelectric materials are integrated in composites to electrically detect mechanical deformations and to exert control actions [6]. Reduced-order modal models are used in the design of active and passive controllers at low and medium frequencies, see among others [2, 3, 9, 14, 15, 17, 23, 30]. In these models, the mechanical states are identified by the time coefficients of a truncated Galerkin approximation on the modal basis. The electric state is specified through the voltages at the electrodes of the piezoelectric transducers. The electromechanical finite-dimensional model is characterized by mechanical mass and stiffness matrices, the coupling matrix between mechanical modes and electric voltages, and an equivalent capacitance matrix.

Modal properties can be identified either numerically or experimentally. Numerical procedures require a suitable structural model and numerical modal analysis methods [18, 20, 29]. Complexity of these procedures sensibly varies according to structure geometry (e.g. beam, plate, and shell) and constitutive behavior. Comprehensive reviews on modeling of structures hosting piezoelectric transducers may be found in [6, 26]. Thorough discussions of finite element solutions are presented in [5]. Experimental methods do not demand complex models and special numerical tools. Nonetheless, the identification of modal parameters requires careful analysis and dedicated techniques.

Most numerical and experimental methods focus on the identification of mechanical properties (resonance frequencies and damping ratios) and of electromechanical couplings [1, 25]. As a matter of fact, they generally discard purely electric properties, that are important for control system design [22] and health monitoring applications [24]. The equivalent piezoelectric capacitance strongly influences the design of active and passive controllers [3, 9, 12, 14, 22, 23] and is fundamental for control electronics and power consumption issues [16]. The piezoelectric capacitance is usually regarded as a property of the piezoelectric elements, furnished in the producers' datasheet. However, as discussed in [21], it is a structural property that depends on the stiffness of the transducer with respect to the stiffness of the host structure. Its values vary with the mechanical conditions imposed on the structure (free or blocked). They may also be affected by the temperature and the applied voltage [19, 28].

To the best of our knowledge, an accurate technique for the identification of the capacitance of reduced order modal models is not available. Also, a thorough discussion of its meaning has not been presented. We study identification methods in reduced-order modal models of linear piezoelectric structures with multiple piezoelectric elements. We focus

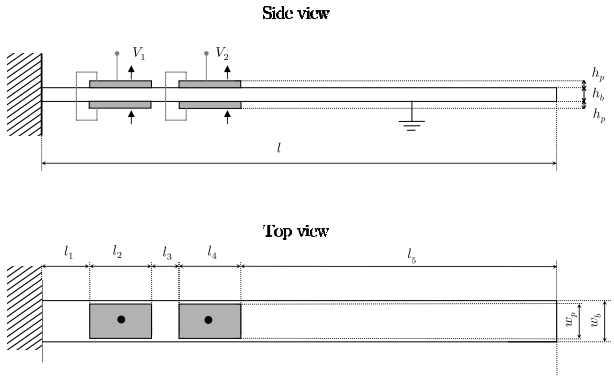

Figure 1. Geometry of the piezoelectric structure considered in the numerical case study and experimental tests.

on the identification of piezoelectric modal couplings and capacitances. We assume that the structural damping is negligible and that the piezoelectric constitutive behavior is linear. The reader can refer to [1, 11, 13, 25] for damping identification and to [16] for the analysis of constitutive non-linearities.

The paper is organized as follows. In section 2, we present the reduced-order modal model of a linear piezoelectric structure. We characterize the piezoelectric capacitance of the modal model. In sections 3 and 4, we present two different experimental identification methods. The former method (OS) is based on the measurement of resonance frequencies of the structure with the piezoelectric transducers either open or short-circuited. The latter method (RS) exploits the properties of the transfer function of the *RL* piezoelectric shunting. In section 5, we consider a specific case study, for which we develop an experimental set-up and a 3D finite element (FE) model. We apply the identification methods on the data obtained by experimental measures and FE numerical results. Their comparison assesses the accuracy of the identification methods and shows the limits of the numerical model and of the measurement techniques. Comments and conclusions are summarized in section 6.

2. Reduced-order models

We consider a linear piezoelectric structure including p piezoelectric transducers. To fix the ideas, we refer to the case study sketched in figure 1 (a cantilever beam hosting two piezoelectric transducers). In this system, each transducer is composed of two thickness polarized sheets of piezoelectric ceramics bonded on both sides of the beam. Each pair of piezoelectric laminae is electrically interconnected in a counter-phase configuration. Thus, an applied voltage results in beam bending.

2.1. Modal equations

We describe the system behavior using the p voltages at the piezoelectric transducers and n modal coordinates. The modal basis consists of the mode shapes of the structures with short-circuited piezoelectric transducers. We assume that the structural damping is negligible. Indices i and j are used for mechanical coordinates and vary between 1 and n. Indices r and s are used for piezoelectric transducers and vary between 1 and p.

The modal coefficients $y_1, \ldots, y_n$ are collected in the n-dimensional vector $\mathbf{y}(t)$, and the piezoelectric voltages $V_1, \ldots V_p$ are grouped in the p-dimensional vector $\mathbf{V}(t)$. We use t to indicate the time variable. The system governing equations in terms of $\mathbf{y}(t)$ and $\mathbf{V}(t)$ are [9, 23]

$$\mathbf{M}\,\ddot{\mathbf{y}}(t) + \mathbf{K}\mathbf{y}(t) - \mathbf{e}\,\mathbf{V}(t) = \mathbf{F}(t) \qquad (1a)$$

$$\mathbf{C}^{\mathbf{y}}\,\mathbf{V}(t) + \mathbf{e}^{\mathsf{T}}\,\mathbf{y}(t) = \mathbf{Q}(t) \qquad (1b)$$

where a superimposed dot means time derivative; a superscripted T indicates matrix transposition; $\mathbf{M}$, and $\mathbf{K}$ are mass and stiffness matrices; $\mathbf{C}^{\mathbf{y}}$ is the piezoelectric capacitance matrix; $\mathbf{e}$ is the piezoelectric coupling matrix; $\mathbf{F}(t)$ represents the mechanical modal forces; $\mathbf{Q}(t)$ collects the total charges $Q_1, \ldots, Q_p$ at the p piezoelectric transducers.

The matrices $\mathbf{M}$, $\mathbf{K}$ and $\mathbf{C}^{\mathbf{y}}$ are diagonal and positive definite. Their non-zero entries are

$$(\mathbf{M})_{ii} = m, \qquad (\mathbf{K})_{ii} = m\omega_i^2, \qquad (\mathbf{C}^{\mathbf{y}})_{rr} = C_r^{\mathbf{y}}$$

where m is the total mass of the system, and the ω_i's are the resonance radian frequencies at constant electric potential ($\mathbf{V}(t) = \bar{\mathbf{V}}$); $C_r^{\mathbf{y}}$ is the capacitance of the rth transducer at constant modal coefficients ($\mathbf{y}(t) = \bar{\mathbf{y}}$). The generic element e_{ir} of $\mathbf{e}$ represents the coupling between the ith mechanical mode and the rth piezoelectric transducer.

2.2. Non-dimensional form

Equations (1*a*) and (1*b*) can be rewritten in non-dimensional form

$$\ddot{\eta}_i + \Omega_i^2\eta_i - \sum_{r=1}^{p}\Omega_i\gamma_{ir}\upsilon_r = \varphi_i, \qquad i = 1, \ldots, n \qquad (2a)$$

$$\upsilon_r + \sum_{i=1}^{n}\Omega_i\gamma_{ir}\eta_i = \chi_r, \qquad r = 1, \ldots, p. \qquad (2b)$$

The non-dimensional radian resonance frequencies and electromechanical couplings appearing in equations (2*a*) and (2*b*) are

$$\Omega_i = \frac{\omega_i}{\omega_0}, \qquad \gamma_{ir} = \frac{e_{ir}}{\omega_i\sqrt{mC_r^{\mathbf{y}}}} \qquad (3)$$

where ω_0 is a scaling radian frequency. The non-dimensional state variables and forcing vectors in equations (2*a*) and (2*b*) are

$$\eta_i = y_i/y_0, \qquad \upsilon_r = V_r/V_{0r},$$

$$\varphi_i = F_i/F_0, \qquad \chi_r = Q_r/Q_{0r}$$

with scaling voltages, forces, and charges given by

$$V_{0r} = \sqrt{\frac{m}{C_r^{\mathbf{y}}}}y_0\omega_0, \qquad F_0 = m\omega_0^2 y_0, \qquad Q_{0r} = V_{0r}C_r^{\mathbf{y}}. \qquad (4)$$

If the mechanical resonance frequencies are sufficiently spaced in the frequency domain, then in the neighborhood of a radian resonance frequency Ω_i the effects of neighboring mechanical modes can be neglected by setting $\eta_j = 0$ for all $j \neq i$.

2.3. Identification problem

Characterization of parameters of equations (2*a*) and (2*b*) requires the identification of

- n short-circuited resonance frequencies ω_i;
- $n \times p$ dimensionless modal couplings e_{ir};
- p electric capacitances $C_r^{\mathbf{y}}$.

The mechanical resonance frequencies ω_i can be identified through standard techniques available for linear elastic structures. We focus on the identification of coupling coefficients e_{ir} and of piezoelectric capacitances $C_r^{\mathbf{y}}$.

2.4. A few comments on the piezoelectric capacitance in the modal model

In classical electrostatics, the capacitance of a two-conductor system is the ratio between the stored charge and the voltage difference between the conductors. It measures the amount of energy stored per unit voltage. In a piezoelectric transducer, the energy has mechanical and electrical contributions. The total energy stored for a given applied voltage depends on the mechanical constraints applied to the piezoelectric element. If the transducer is blocked, the elastic energy is kept constant and the external work done by the applied potential is stored only in the electric form. If the piezoelectric transducer is free, part of the work exerted by the applied potential is stored in the mechanical form. This results in an increase of piezoelectric capacitance. In the theory of the 3D piezoelectricity [4], this fact motivates the distinction between the electric permittivity at constant stress ε^{T} and at constant deformation ε^{S}.

For a stand-alone piezoelectric transducer made of a sheet of thickness-polarized piezoelectric ceramics, the capacitances associated to ϵ^{T} and ϵ^{S} are the *free capacitance*:

$$C_r^{\mathrm{T}} = \frac{\varepsilon_{33}^{\mathrm{T}} A}{H}, \tag{5}$$

and the *blocked capacitance*

$$C_r^{\mathrm{S}} = \frac{\varepsilon_{33}^{\mathrm{S}} A}{H},$$

where A is the surface of the electrodes, H is the thickness of the transducer, and 3 is the index associated with the direction of polarization (thickness). For common piezoelectric materials (e.g. PZT-5H) the percentile difference between C^{T} and C^{S} is as high as 40%.

The capacitance of a piezoelectric element bonded on or embedded in a structure is neither C^{T} nor C^{S}. The host structure partially impedes the deformation of the piezoelectric element. The value of the modal capacitance depends on the relative stiffness of the host structure and the piezoelectric element [21]. It ranges between the blocked and the free capacitances. As is customary for 3D piezoelectricity, for the modal model in equations (1*a*) and (1*b*) we must also distinguish between two capacitances:

- The *free modal capacitance* $C_r^{\mathbf{F}}$, measured when the structure is left free to deform (superscript **F** refers to constant external forces).
- The *blocked modal capacitance* $C_r^{\mathbf{y}}$, measured when the modal coefficients **y** are blocked.

In the technical literature different authors use different capacitances for the modal representation in equations (1*a*) and (1*b*). Among others [12, 14], and [18] estimates $C_r^{\mathbf{y}}$ with the capacitance of the stand-alone piezoelectric transducer at constant stress, C^{T}; while [23] retains the value measured by an impedance analyser for the structure free to deform, $C_r^{\mathbf{F}}$. However, the analysis of equations (1*a*) and (1*b*) shows that $C_r^{\mathbf{y}}$ is the ratio between the charge and voltage for blocked modal coordinates. Unfortunately, the direct measurement of $C_r^{\mathbf{y}}$ is difficult, because it requires blocking all the modal deflections. Vice versa, $C_r^{\mathbf{F}}$ can be easily measured using a multimeter or an impedance analyser between the electric terminals of the transducer and leaving the structure free to deform. Techniques for the estimate of $C_r^{\mathbf{y}}$ are discussed in sections 3 and 4.

3. Identification by open/short-circuit frequencies and free capacitances (OS method)

The non-dimensional piezoelectric coupling coefficients γ_{ir} may be determined by the identification method used in [14], which builds on the effect of the electric coupling on the mechanical stiffness. We apply this technique, denoted here as the OS method (open-circuit/short-circuit), to estimate also the piezoelectric capacitance $C_r^{\mathbf{y}}$. This is done by measuring the free modal capacitance $C_r^{\mathbf{F}}$ and the coupling coefficients γ_{ir}.

3.1. Coupling coefficient

In the OS method, each γ_{ir} is identified from the radian resonance frequency $\Omega_i = \omega_i/\omega_0$ of the structure with every transducer short-circuited, and the radian resonance frequency $\mathring{\Omega}_i^{(r)} = \mathring{\omega}_i^{(r)}/\omega_0$ of the structure with every transducer short-circuited except the rth one left open-circuited. We assume that the mechanical resonance frequencies are reasonably spaced in the frequency axis. This implies that the influence of the jth mode on the mode ith can be neglected for $j \neq i$. From equations (2*a*) and (2*b*) with $\chi_r = 0$, the radian frequency $\mathring{\Omega}_i^{(r)}$ is calculated

$$\mathring{\Omega}_i^{(r)} = \Omega_i \sqrt{1 + \gamma_{ir}^2}.$$

Thus, the coupling coefficient is estimated by

$$|\gamma_{ir}| = \sqrt{\left(\frac{\mathring{\omega}_i^{(r)}}{\omega_i}\right)^2 - 1}. \tag{6}$$

If the radian frequencies are measured with an uncertainty σ_ω, the uncertainty of the coupling estimate is

$$\frac{\sigma(|\gamma_{ir}|)}{|\gamma_{ir}|} = \frac{1}{|\gamma_{ir}|}\sqrt{\left(\frac{d|\gamma_{ir}|}{d\mathring{\omega}_i^{(r)}}\right)^2 + \left(\frac{d|\gamma_{ir}|}{d\omega_i}\right)^2}\sigma_\omega$$
$$= \frac{1}{|\gamma_{ir}|\omega_0}\sqrt{\frac{(\omega_i)^2 + (\mathring{\omega}_i^{(r)})^2}{(\mathring{\omega}_i^{(r)})^2 - (\omega_i)^2}}\sigma_\omega \simeq \frac{\sqrt{2}}{\gamma_{ir}^2}\frac{\sigma_\omega}{\omega_i}. \tag{7}$$

The last approximation in (7) holds for small coupling. In structures hosting multiple piezoelectric elements, the coupling coefficient of a single transducer is usually very small (typically $\gamma_{ir} \sim 0.01$–0.3). Thus, the estimate of γ in (7) is very sensitive to errors in the resonance frequencies.

From the identified non-dimensional coupling, the dimensional coefficient e_{ir} is found from equation (3) as

$$e_{ir} = \omega_i \gamma_{ir} \sqrt{m C_r^{\mathbf{y}}}. \tag{8}$$

Evaluation of e_{ir} in equation (8) requires the blocked modal capacitance $C_r^{\mathbf{y}}$.

3.2. Piezoelectric capacitance

We compute a relation between the free modal capacitance $C_r^{\mathbf{F}}$ and the blocked modal capacitance $C_r^{\mathbf{y}}$ by considering the static version of equations (1*a*) and (1*b*)

$$\mathbf{K}\,\mathbf{y} - \mathbf{e}\,\mathbf{V} = \mathbf{F} \tag{9a}$$

$$\mathbf{C}^{\mathbf{y}}\,\mathbf{V} + \mathbf{e}^{\mathsf{T}}\,\mathbf{y} = \mathbf{Q}. \tag{9b}$$

Assuming that the modal forces are zero, and eliminating the static modal displacement $\mathbf{y}$ in equations (9*a*) and (9*b*), we obtain

$$\frac{Q_r}{V_r} = C_r^{\mathbf{y}} + \frac{1}{m}\sum_{j=1}^{n} \frac{e_{jr}^2}{\omega_j^2}. \tag{10}$$

By definition, the left-hand side of equation (10) is the free modal capacitance of the rth transducer. Thus using the definition of the non-dimensional couplings in equation (3), we have that the blocked and the free modal capacitances of the rth transducer are related by

$$C_r^{\mathbf{y}} = \frac{C_r^{\mathbf{F}}}{1 + \sum_{j=1}^{n} \gamma_{jr}^2}. \tag{11}$$

4. Identification by resonant shunting (RS method)

Consider a piezoelectric structure where a piezoelectric transducer, say the rth one, is shunted with an impedance comprised of an inductor L and a resistor R in parallel connection. This is the so-called resonant shunted piezoelectric transducer, used in vibration control applications to electrically absorb mechanical energy [2, 9, 14, 23]. Assume that a different piezoelectric transducer, say the ath one, is driven by a prescribed voltage $\bar{\upsilon}$, and that all the other transducers are short-circuited. As we have done in section 3, about each radian resonance frequency ω_i, we model the system with a single mechanical degree of freedom by setting $n = 1$ and $\mathbf{y} = y_i$. Defining the flux linkage ψ_r as $\dot{\psi}_r = \upsilon_r$, equations (2*a*) and (2*b*) become

$$\ddot{\eta}_i + \Omega_i^2 \eta_i - \Omega_i \gamma_{ir} \dot{\psi}_r = \Omega_i \gamma_{ia} \bar{\upsilon} \tag{12a}$$

$$\ddot{\psi}_r + \Omega_i^2 \beta \psi_r + \Omega_i \delta \dot{\psi}_r + \Omega_i \gamma_{ir} \dot{\eta}_i = 0 \tag{12b}$$

where β and δ are given by

$$\beta = \frac{1}{\omega_i^2 L C_r^{y_i}}, \qquad \delta = \frac{1}{\omega_i R C_r^{y_i}}. \tag{13}$$

We note that the capacitance $C_r^{y_i}$ is the blocked modal capacitance of the rth transducer resulting from the one d.o.f. model in equations (12*a*) and (12*b*). The parameters β and δ in equation (13) are the electric tuning and damping and they depend on the inductance and the resistance. The system modal mobility function, defined as the ratio between the Fourier transforms of the modal velocity $\dot{\eta}_i$ and the modal force $\Omega_i \gamma_{ia} \bar{\upsilon}$, is

$$H(\beta, \delta, \Omega) = \mathrm{i}\Omega\,\Omega_i^2 \times \frac{\beta - \Omega^2 + \mathrm{i}\Omega\delta}{\Omega^4 - \mathrm{i}\Omega^3\delta - \Omega^2(\beta + 1 + \gamma_{ir}^2) + \mathrm{i}\Omega\delta + \beta}$$

where $\Omega = \omega/\omega_0$ is the non-dimensional radian frequency and i is the imaginary unit.

When β tends to infinity (meaning that $L \to 0$), $H(\infty, \delta, \Omega)$ is the mobility function corresponding to the case where the rth transducer is short-circuited. It is possible to show (see [9, 10, 14]) that the absolute values of $H(\beta, \delta, \Omega)$ and $H(\infty, \delta, \Omega)$ for any value of δ intersect at two points $S = (\Omega_{\mathrm{S}}, |H_{\mathrm{S}}|)$ and $T = (\Omega_{\mathrm{T}}, |H_{\mathrm{T}}|)$, and that the two amplitudes $|H_{\mathrm{S}}|$ and $|H_{\mathrm{T}}|$ are equal when

$$\beta = 1 \Rightarrow L = \frac{1}{\omega_i^2 C_r^{y_i}}. \tag{14}$$

Equation (14) implies that $|H_{\mathrm{S}}| = |H_{\mathrm{T}}|$ when the electric circuit composed of the inherent piezoelectric capacitance and the shunting inductance is tuned at the mechanical resonance. Furthermore, when condition (14) is satisfied,

$$\frac{\Omega_{\mathrm{T}} - \Omega_{\mathrm{S}}}{\Omega_i} = \frac{\omega_{\mathrm{T}} - \omega_{\mathrm{S}}}{\omega_i} = \frac{|\gamma_{ir}|}{\sqrt{2}}.$$

Therefore, after adjusting the inductance to accomplish the tuning condition on the amplitude of the S and T points, the measurement of the corresponding values of L, ω_{T}, ω_{S} and ω_i allow for the simultaneous estimate of the modal coupling coefficient and the piezoelectric capacitance through the following relations:

$$|\gamma_{ir}| = \sqrt{2}\,\frac{\omega_{\mathrm{T}} - \omega_{\mathrm{S}}}{\omega_i} \tag{15a}$$

$$C_r^{y_i} = \frac{1}{L\omega_i^2} = \frac{1}{4\pi^2 f_i^2 L} \tag{15b}$$

where f_i is the ith resonance frequency.

Parasitic electric losses do not influence the method, since the absolute value of the mobility function passes through the S and T points independently of the value of R [9, 10, 14].

If the frequencies are measured with an uncertainty σ_ω, the uncertainty of the estimated coupling is

$$\frac{\sigma(|\gamma_{ir}|)}{|\gamma_{ir}|} = \left(\sqrt{\frac{4}{\gamma_{ir}^2} + 1}\right)\frac{\sigma_\omega}{\omega_0} \simeq \frac{2}{|\gamma_{ir}|}\frac{\sigma_\omega}{\omega_0} \tag{16}$$

where the last approximation holds only for small coupling.

4.1. A few comments on the influence of the number of modes on the modal model parameters

In order to establish a relation between the capacitance $C_r^{y_i}$ resulting from the RS identification method and the blocked modal capacitance $C_r^{\mathbf{y}}$ characterizing the n-mode model in equations (1*a*) and (1*b*) we refer again to the static model in equations (9*a*) and (9*b*). Assuming that $F_j = 0$ for $j \neq i$, equations (9*a*) and (9*b*) give

$$C_r^{\mathbf{y}} V_r + e_{ir} y_i + \sum_{j \neq i} \sum_{s} \frac{e_{jr}}{m\omega_j^2} e_{js} V_s = Q_r. \tag{17}$$

Table 1. Dimensions of the beam and the piezoelectric elements.

Dimensions (mm)				
$l_1 = 5.0$	$l_2 = 36.5$	$l_3 = 6.0$	$l_4 = 36.5$	$l_5 = 117.0$
$l = 201.0$	$w_p = 17.6$	$w_b = 20$	$h_p = 0.267$	$h_b = 2.85$

The capacitance $C_r^{y_i}$ is the ratio Q_r/V_r in equation (17) with $V_s = 0$ for all $s \neq r$ and $y_i = 0$

$$C_r^{y_i} = C_r^{\mathbf{y}} + \sum_{j\neq i} \frac{e_{jr}^2}{m\omega_j^2} = C_r^{\mathbf{y}}\left(1 + \sum_{j\neq i} \gamma_{jr}^2\right). \qquad (18)$$

Equation (18) implies that the capacitance of the one-mode model is larger than the capacitance of the n-mode model.

From equation (18) we can estimate the dimensional modal coupling e_{ir} from the dimensionless modal coupling γ_{ir} by using equation (3)

$$e_{ir} = \omega_i \gamma_{ir} \sqrt{m C_r^{\mathbf{y}}} = \frac{\gamma_{ir}}{\sqrt{1 + \sum_{j\neq i} \gamma_{jr}^2}} \omega_i \sqrt{m C_r^{(y_i)}}. \qquad (19)$$

Equations (18) and (19) allow us to calculate the parameters of a n-mode model from the knowledge of the coupling coefficients γ_{ir} and the capacitance $C_r^{(y_i)}$ obtained with the one-mode approximation in the RS identification procedure. These additional steps are not required by the OS method, that provides directly the capacitance $C_r^{\mathbf{y}}$ from (11).

5. Case study

We apply the identification methods of sections 3 and 4 to the beam in figure 1 with the geometrical and material properties listed in tables 1 and 2. We compare experimental findings with numerical results from 3D finite element (FE) analysis.

Experimental identification of the resonance frequency, couplings, and piezoelectric capacitances is made by using both the OS and the RS methods. We identify the parameters of a reduced-order modal model with one mechanical degree of freedom representing the deflection on the lowest bending mode and the two voltages of the transducers.

The parameters of the same modal model are identified by applying the OS method to FE analysis with the commercial code ABAQUS 6.5. Comparison between experimental and numerical results is helpful for understanding the limits of theoretical models, and for assessing the accuracy of the identification methods. In the FE model, we also compute the blocked modal capacitance of the two transducers using a four-modes model, in order to provide a better picture of the sensitivity of the modal capacitance on the order of the modal reduction.

5.1. Description

5.1.1. Experimental set-up. A cantilever aluminum beam (Al6061-T6) hosting two surface bonded bimorph pairs of piezoelectric transducers (Piezo-System T110-H4E-602) was built (see figure 2). The piezoelectric elements were bonded on the beam by a thin layer of non-conductive epoxy resin and each bimorph pair was electrically interconnected in parallel

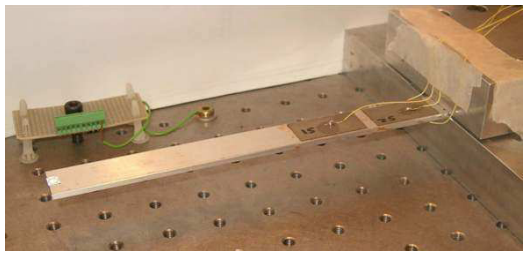

Figure 2. Cantilever beam with piezoelectric transducers used for experimental tests.

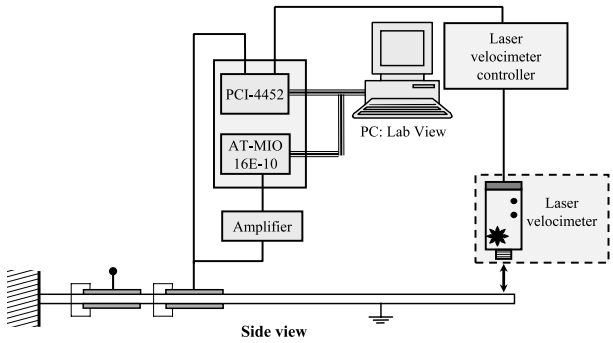

Figure 3. Experimental set-up for frequency response measurement.

and counter-phase. A single piezoelectric element is made of a layer of thickness-polarized piezoelectric ceramic (PZT-5H) having the upper and lower surfaces covered by a thin nickel film serving as electrode. The electric contact between the lower electrode of each transducer and the grounded beam was achieved by applying a small spot of electrically conductive adhesive at the central region of the piezoelectric transducer, where interfacial stresses are low [7].

The beam frequency response was determined by exciting the structure with a frequency sweep signal at one of the two piezoelectric pairs and measuring the beam tip velocity by a laser velocimeter (Polytec OFV 350) as illustrated in figure 3. The input signal was digitally generated in Labview, converted by the D/A converter National Instruments AT-MIO-16E-10, and amplified by an ad hoc designed voltage amplifier. The analog output of the laser and the voltage applied at the exciting transducer were measured by the A/D converter National Instruments PCI-4452, and a personal computer was used for digital signal processing. Non-invasive measurements were performed by exciting the beam with one of the surface-bonded transducers, and by measuring the tip velocity with the laser vibrometer.

The RS identification method requires a high-value adjustable inductor. An inductor with these characteristics was simulated by exploiting the two operational amplifiers RC circuit depicted in figure 4, which is a modified Antoniou circuit [27]. The corresponding equivalent inductance L is given as a function of the circuital components by

$$L = \frac{R_1 R_4 R_6}{R_2} C_5.$$

The resistance R_3 adds a series negative resistance that can be exploited to cancel parasitic losses [27]. FET-input operational

Table 2. Material data for aluminum and piezoelectric ceramics.

Aluminum (Al6061-T6)		
$\rho_V^{(\mathrm{al})} = 2700\ \mathrm{kg\ m^{-3}}$,	$Y^{(\mathrm{al})} = 69 \times 10^9\ \mathrm{N\ m^{-2}}$,	$\nu^{(al)} = 0.33$
Piezoelectric ceramics (PZT-5H-S4-ENH)		
$\rho_V^{(\mathrm{PZT})} = 7800\ \mathrm{kg\ m^{-3}}$,	$Y_1^{(\mathrm{PZT})} = 62 \times 10^9\ \mathrm{N\ m^{-2}}$,	$Y_3^{(\mathrm{PZT})} = 50 \times 10^9\ \mathrm{N\ m^{-2}}$
$\nu_{12} = 0.31$,	$d_{31} = -320 \times 10^{-12}\ \mathrm{m\ V^{-1}}$,	$d_{33} = 650 \times 10^{-12}\ \mathrm{m\ V^{-1}}$
$\varepsilon_{33}^{\mathrm{T}} = 3800\varepsilon_0$		

Table 3. First four resonance frequencies ($f = \omega/2\pi$) of the beam with short-circuited piezoelectric transducers. Comparisons between experimental and FE results.

	f_1 (Hz)	f_2 (Hz)	f_3 (Hz)	f_4 (Hz)
Experimental	66.25	360.2	990	1943
3D FE	66.97(+1.09%)	365.6(+1.50%)	1005.2(+1.53%)	1960.5(+0.90%)

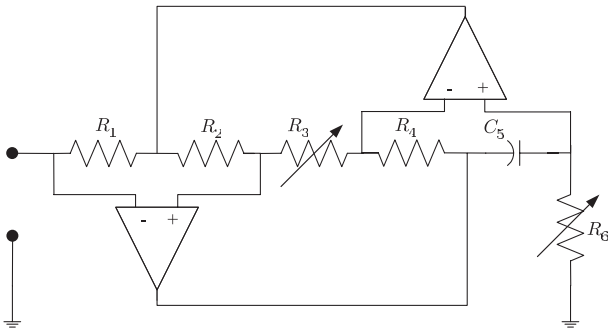

Figure 4. Schematics of the simulated adjustable inductance (modified Antoniou circuit).

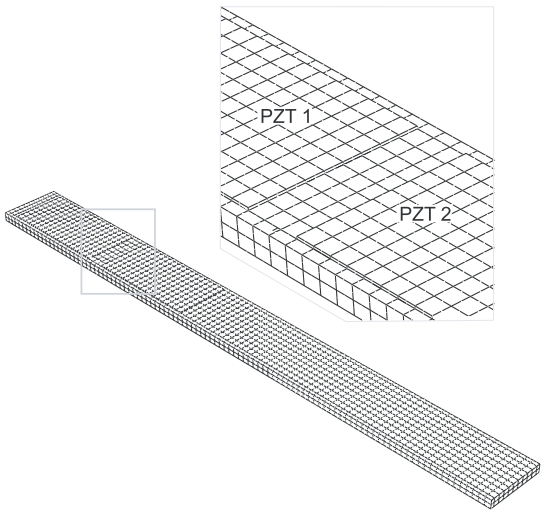

Figure 5. Finite element mesh.

amplifiers Burr-Brown OPA445AP operated at high voltages by a dual output power supply TTi EX752M at ±30 V and high-precision resistors (±1%) were used.

We note that the main source of nonlinearities can be attributed to the non-ideal behavior of the capacitor C_5. To obtain a linear behavior at low frequencies, we used a non-polarized polyester capacitor.

5.1.2. Finite element model. Numerical simulations for the structure in figure 1 were performed by using the FE commercial code ABAQUS 6.5. The FE model uses 3D brick 20-node elements with quadratic shape functions and reduced integration (elements C3D20R for the elastic part and C3D20RE for the piezoelectric part). The piezoelectric elements have four degrees of freedom per node, the three components of the mechanical displacement and the electric potential. The piezoelectric surfaces covered by the electrodes are modeled by constraining the electric potential of the associated nodes to a single value, that is the electrode potential. The electric interconnections between the piezoelectric transducers bonded on the upper and lower faces of the structure are obtained by constraining the corresponding electrode potentials. Short-circuit or open-circuit conditions are simulated by setting to zero or leaving free the electrode voltage difference. The piezoelectric laminae and the elastic beam are assembled by constraining the relative displacement at the interface, according to the perfect bonding assumption. The use of quadratic elements allows us to get a good convergence of the FE results with a limited number of elements through the thickness of the elastic part and the piezoelectric laminae. This is particularly important for the computational cost. After refinement essays, the adopted mesh includes a single element through the thickness of the piezoelectric transducers and two elements along the thickness of the elastic beam (see figure 5). The total number of elements is 2870, the total number of nodes is 18 212 and the total number of variables in the FE model is 59 720.

5.2. Results

5.2.1. Resonance frequencies and frequency response with the shunt circuit. In table 3 we compare experimental and FE results for the first four resonance frequencies of the beam with short-circuited piezoelectric elements. Table 4 reports the lowest bending frequency obtained when one of the two piezoelectric elements is open-circuited. Data in table 4 are required for the identification of the coupling coefficients with the OS method.

Figures 6 and 7 show the experimental mobility functions measured when shunting one of the piezoelectric elements with

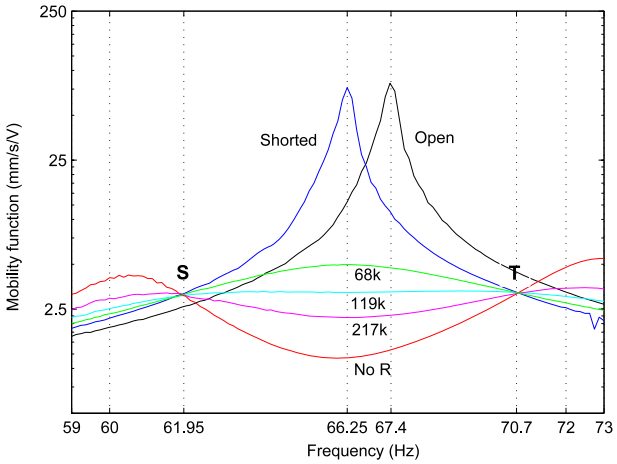

Figure 6. Experimental mobility function of the stepped beam in figures 1 and 2 obtained by exciting the structure at the second transducer and either shunting the first with the adjustable inductor and different resistors, or leaving it open/short-circuited. The inductance is tuned to set the electric resonance to the first mechanical resonance frequency.

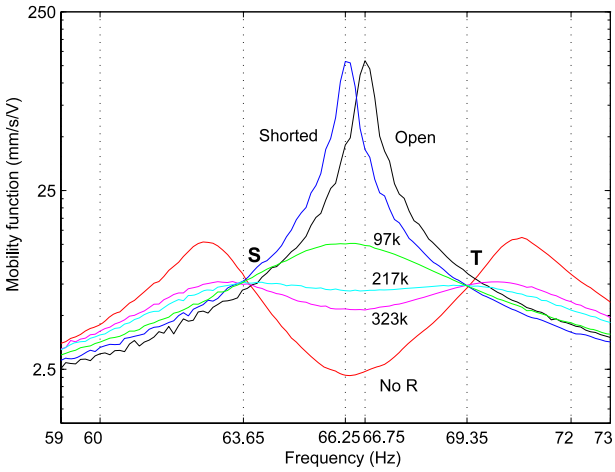

Figure 7. Experimental mobility function obtained by exciting the structure at the first transducer and either shunting the second with the adjustable inductor and different resistors, or leaving it open/short-circuited.

Table 4. First resonance frequency when one or both of the transducers are short-circuited, where $\mathring{f}_i^{(r)} = \mathring{\omega}_i^{(r)}/2\pi$ (see section 3.1). Comparisons between experimental and FE results.

	f_1 (Hz) ($V_1 = 0$, $V_2 = 0$)	$\mathring{f}_1^{(1)}$ (Hz) ($\dot{Q}_1 = 0$, $V_2 = 0$)	$\mathring{f}_1^{(2)}$ (Hz) ($V_1 = 0$, $\dot{Q}_2 = 0$)
Experimental	66.25	67.40	66.75
3D FE	66.97	68.52	67.57

Table 5. Experimental results for the frequencies and the inductances required by the RS identification method (see equations (15*a*) and (15*b*)).

	f_S (Hz)	f_T (Hz)	f_1 (Hz)	L (H)
Shunt on PZT 1	61.95	70.70	66.25	57.6
Shunt on PZT 2	63.65	69.35	66.25	58.1

a parallel RL circuit. Figure 6 is obtained by shunting the first piezoelectric element and by exciting the beam with the second one. Figure 7 corresponds to the opposite situation (excitation on the first and shunting on the second). In the two cases, the adjustable inductor of the shunting circuit is tuned to get the same amplitude of the frequency response at the S and T fixed points. Each plot reports the frequency response for a different value of the resistor. Table 5 summarizes the experimental findings on the resonant shunting. Data in table 5 are required by the RS identification method.

5.2.2. Coupling coefficients. The non-dimensional piezoelectric coupling between the first beam mode and the two transducers are identified with the RS and the OS methods. The coefficients found by using equations (15*a*) and (6), are reported in table 6. The experimental results of the RS and the OS methods are very close. However, the errors with respect to the numerical estimates are not negligible (∼10%). The difference between the experimental and FE results suggests to include

Table 6. Coupling coefficients of the piezoelectric transducers experimentally identified with the OS and RS methods, and numerically identified with the OS method. Percentile differences with respect to the numerical results are in parentheses.

	Experimental		3D FE
	RS—(15*a*)	OS—(6)	OS—(6)
γ_{11}	0.187(−13.5%)	0.184(−14.9%)	0.216
γ_{12}	0.122(−9.21%)	0.122(−9.21%)	0.142

the effect of the bonding layer to improve the estimate of the coupling coefficients [7, 8, 29]. However, this is difficult in practice because of the uncertainties on the data about bonding layer thickness and stiffness.

5.2.3. Capacitances. As explained in section 2.4, the value of the piezoelectric capacitance depends on the mechanical conditions under which the measurement is done. The value reported in the datasheet of the piezoelectric elements is the free capacitance $C^T = 152$ nF in equation (5). The difference between this value and the modal capacitances is significant (∼50%). Table 7 reports the results for the capacitances $C_1^{y_1}$ and $C_2^{y_1}$ of the modal representation including only the first beam bending mode. The experimental values obtained using the RS and the OS methods are compared with results from the application of the OS method to the numerical model.

The FE results and the experimental findings achieved with the RS method are in close agreement. On the other hand, the free modal capacitance measured using a multimeter is larger than the free capacitance given by the FE model. In our opinion, this is due to the inaccuracy of the capacitance measured with a multimeter. For this reason, the RS method seems preferable for the experimental estimate of the modal capacitance. Comparison of the finite element capacitances of modal model with $n = 1$ and 4 modes assesses the dependence of the capacitance on the number of modes (see section 2.4). Experimental results are for $n = 1$.

Table 7. Piezoelectric capacitances. Percentile errors in parentheses are with respect to the modal capacitance $C_r^{y_1}$ resulting from the OS method applied to the numerical model. The blocked capacitance of the standing-alone piezoelectric transducer is $C^{\mathrm{T}} = 152$ nF.

	Experimental			3D FE		
	$C_r^{\mathbf{F}}$	RS $C_r^{y_1}$—(15*b*)	OS ($n = 1$) $C_r^{y_1}$—(11)	$C_r^{\mathbf{F}}$	OS ($n = 1$) $C_r^{y_1}$—(11)	OS ($n = 4$) $C_r^{\mathbf{y}}$—(11)
PZT 1	114 nF (+13.7%)	100 nF (−0.3%)	110.3 nF (+10.0%)	105.0 nF (+4.7%)	100.3 nF —	95.5 nF (−4.8%)
PZT 2	112 nF (+8.3%)	99 nF (−4.2%)	110.4 nF (+6.8%)	105.3 nF (+1.8%)	103.4 nF —	100.1 nF (−3.2%)

6. Conclusions

We studied experimental identification of mechanical, electric, and coupling coefficients in modal models of linear piezoelectric structures. We proposed two tractable methods based on simple vibration tests. The first method (OS) is based on measuring the resonance frequencies of the structure with piezoelectric transducers open- or short-circuited. The second method (RS) makes use of the piezoelectric shunting and requires an adjustable inductor. Their features are summarized in table 8. The two identification methods can be easily implemented either in experimental set-ups or finite element models, without the need of time-consuming post-processing or dedicated system identification routines.

We commented on the problem of properly identifying the piezoelectric capacitance of the modal representation. We clarified the dependence of the modal capacitance on the mechanical constraints imposed on the structure and on the number of modes included in the model. We showed that the capacitance of the modal model may significantly differ from the nominal capacitance of the standing-alone piezoelectric transducer that is assumed as the correct capacitance by many authors. This percentile difference is as high as 50% in the considered case study (a beam with two bimorph pairs of piezoelectric transducers). The modal capacitance is also different from the capacitance measured when leaving the structure free to deform and depends on the order of the modal model. Nevertheless, these differences are relatively smaller. For the considered case study the percentile errors are about 5%.

Comparison between the results obtained from finite elements and the experimental data underlines the limits of the numerical model and of the measurement techniques. On the one hand, the finite element model, by neglecting the finite stiffness and thickness of the bonding layer, overestimates the electromechanical couplings. On the other hand, the static measure of the capacitance obtained with a multimeter seems to be inaccurate with respect to the estimate of the RS method, which is in close agreement to finite element results. The OS method appears useful and accurate, especially for identification performed from the finite element analysis; the RS method is proved to be preferable for the experimental identification (more accurate coupling and capacitance estimates). A natural development of the present work is the introduction of structural damping and material non-linearities in the modal model and the consequent extension of the proposed identification method.

Table 8. Comparisons between the two identification methods.

	OS method	RS method
Required data	ω_i, $\mathring{\omega}_i^{(r)}$, $C^{\mathbf{F}}$	ω_i, ω_{S}, ω_{T}, L
Couplings γ_{ir}	$\sqrt{(\mathring{\omega}_i^r/\omega_i)^2 - 1}$	$\sqrt{2}(\omega_{\mathrm{T}} - \omega_{\mathrm{S}})/\omega_i$
Capacitance $C_r^{y_i}$	$C^{\mathbf{F}}/(1 + \gamma_{ir}^2)$	$1/\omega_i^2 L$
Advantages	Experimentally and numerically tractable	Accurate
Disadvantages	Relatively imprecise	Requires a synthetic inductor

Acknowledgments

The present work has been carried out in the framework of the joint research project 'Smart materials and structures: structural control using distributed piezoelectric transducers and passive electric networks' funded by the international agreement between CNRS (France) and CNR (Italy), project no. 16283. The authors would also like to acknowledge Professor A Sestieri for offering them access to the Mechanical Vibrations Laboratory of the University of Rome 'La Sapienza'.

References

[1] Agneni A and Coppotelli G 2004 Modal parameter prediction for structures with resistive loaded piezoelectric devices *Exp. Mech.* **44** 97–100

[2] Andreaus U, dell'Isola F and Porfiri M 2004 Piezoelectric passive distributed controllers for beam flexural vibrations *J. Vib. Control* **10** 625–59

[3] Andreaus U and Porfiri M 2006 Effect of electrical uncertainties on resonant piezoelectric shunting *J. Intell. Mater. Syst. Struct.* doi:10.1177/1045389X06067116

[4] ANSI/IEEE std 176-1987, IEEE Standard on Piezoelectricity, 1988

[5] Benjeddou A 2000 Advances in piezoelectric finite element modeling of adaptive structural elements: a survey *Comput. Struct.* **76** 347–63

[6] Chopra I 2002 Review of state of art of smart structures and integrated systems *AIAA J.* **40** 2145–87

[7] Crawley E F and de Luis J 1987 Use of piezoelectric actuators as elements of intelligent structures *AIAA J.* **25** 1373–85

[8] de Faria A R 2003 The impact of finite-stiffness bonding on the sensing effectiveness of piezoelectric patches *Smart Mater. Struct.* **12** N5–8

[9] dell'Isola F, Maurini C and Porfiri M 2004 Passive damping of beam vibrations through distributed electric networks and piezoelectric transducers: prototype design and experimental validation *Smart Mater. Struct.* **13** 299–308

[10] Den Hartog J P 1956 *Mechanical Vibration* (New York: McGraw-Hill)
[11] Duigou L, Daya E M and Potier-Ferry M 2006 Equivalent stiffness and damping of sandwich piezoelectric beams submitted to active control *Smart Mater. Struct.* **15** 623–30
[12] Fleming A J, Behrens S and Moheimani S O 2003 Reducing the inductance requirements of piezoelectric shunt damping systems *Smart Mater. Struct.* **12** 57–64
[13] Gaudenzi P, Carbonaro R and Benzi E 2000 Control of beam vibrations by means of piezoelectric devices: theory and experiments *Compos. Struct.* **50** 373–9
[14] Hagood N W and von Flotow A 1991 Damping of structural vibrations with piezoelectric materials and passive electrical networks *J. Sound Vib.* **146** 243–68
[15] Hanagud S, Obal M W and Calise A J 1992 Optimal vibration control by the use of piezoceramic sensors and actuators *J. Guid. Control Dyn.* **15** 1199–206
[16] Jordan J, Ounaies Z, Tripp J and Tcheng P 2000 Electrical properties and power considerations of a piezoelectric actuator *ICASE Report 2000-8* NASA/CR-2000-209861
[17] Kim J, Tyu Y H and Choi S B 2000 New shunting parameter tuning method for piezoelectric damping on measured electrical impedance *Smart Mater. Struct.* **9** 868–77
[18] Kusculuoglu Z K, Fallahi B and Royston T J 2004 Finite element model of a beam with a piezoceramic patch actuator *J. Sound Vib.* **276** 27–44
[19] Law W W, Liao W H and Huang J 2003 Vibration control of structures with self-sensing piezoelectric actuators incorporating adaptive mechanisms *Smart Mater. Struct.* **12** 720–30
[20] Maurini C, Porfiri M and Pouget J 2006 Numerical methods for modal analysis of stepped piezoelectric beams *J. Sound Vib.* **298** 918–33
[21] Maurini C, Pouget J and dell'Isola F 2006 Extension of the Euler–Bernoulli model of piezoelectric laminates to include 3D effects via a mixed approach *Comput. Struct.* **84** 1438–58
[22] Moheimani S O R and Fleming A J 2006 *Piezoelectric Transducers for Vibration Control and Damping* (New York: Springer)
[23] Park C H 2003 Dynamics modelling of beams with shunted piezoelectric elements *J. Sound Vib.* **268** 115–29
[24] Park G, Sohn H, Farrar C R and Inman D J 2003 Overview of piezoelectric impedance-based health monitoring and path forward *Shock Vib. Digest* **35** 451–63
[25] Saunders W R, Cole D G and Robertshaw H H 1994 Experiments in piezostructure modal analysis for MIMO feedback control *Smart Mater. Struct.* **3** 210–8
[26] Saravanos D A and Heyliger P R 1996 Mechanics and computational models for laminated piezoelectric beams, plates, and shells *Appl. Mech. Rev.* **52** 305–20
[27] Senani R 1996 Alternative modification of the classical GIC structure *Electron. Lett.* **32** 1329
[28] Vipperman J S and Clark R L 1996 Implementation of an adaptive piezoelectric sensoriactuator *AIAA J.* **34** 2102–9
[29] Yang S M and Lee Y J 1994 Interaction of structure vibration and piezoelectric actuation *Smart Mater. Struct.* **3** 494–500
[30] Zhang N and Kirpitchenko I 2002 Modelling the dynamics of a continuous structure with a piezoelectric sensor/actuator for passive structural control *J. Sound Vib.* **249** 251–61